

Article

Physical Model for Frequency Domain Spectroscopy of Oil–Paper Insulation in a Wide Temperature Range by a Novel Analysis Approach

Jiacheng Xie * , Ming Dong, Boning Yu, Yizhuo Hu, Kaige Yang and Changjie Xia 

State Key Laboratory of Electrical Insulation for Power Equipment, Xi'an Jiaotong University, Xi'an 710049, China; dongming@xjtu.edu.cn (M.D.); yuboning@stu.xjtu.edu.cn (B.Y.); h1375776307@stu.xjtu.edu.cn (Y.H.); ykg870995750@stu.xjtu.edu.cn (K.Y.); xcj19960521@stu.xjtu.edu.cn (C.X.)

* Correspondence: xiejiacheng@stu.xjtu.edu.cn; Tel.: +86-1862-919-9914

Received: 6 August 2020; Accepted: 31 August 2020; Published: 1 September 2020



Abstract: Frequency domain spectroscopy is considered to be a promising and novel method for the assessment of the insulation condition of power equipment. This work has practical significance as it explains the microscopic mechanism of this method in a wide temperature range and further establishes its quantitative model. To achieve this, in the present paper, we select oil-impregnated paper—one of the most common insulation materials for power equipment with a complex microstructure—as a test sample, deduce a formula based on the relationship between the real and imaginary parts of the complex permittivity to extract the spectra of independent dielectric processes and measure the frequency domain spectra of oil-impregnated paper under different temperatures, as well as its thermally stimulated depolarization current with a series of bias voltages. The analysis results reveal that oil-impregnated paper's frequency domain spectra in a wide temperature range are mainly determined by dielectric processes whose generation mechanisms are low-frequency dispersion, DC conduction, electrode relaxation, interfacial relaxation and dipole relaxation, respectively. Moreover, due to the different thermal properties of charge motions, the macroscopic characteristics and microscopic generation mechanisms of both spectra vary significantly with the sample's temperature. After verifying the generation mechanisms of the spectra in high, middle and low-temperature ranges, function models for those spectra with clear physical meanings are established separately, providing sufficient physical parameters to carry out insulation assessment.

Keywords: insulation condition assessment; frequency domain spectroscopy; relaxation and conduction; wide temperature range

1. Introduction

As the basic unit of a power system, power equipment adopts various dielectric materials for insulation purposes when operating under high-voltage conditions [1]. Among these materials, oil-impregnated paper, which simultaneously benefits from the advantages of the high insulating strength of solid polymers and the excellent heat dissipation of liquids, is considered to be an ideal form of insulation in core equipment such as power transformers, bushing and power cables [2]. The typical structure of the cellulose macromolecule chain is presented in Figure 1 [3]. For decades, with the aim of providing reliable advice on maintenance decisions for power equipment and effectively ensuring power supply safety, extensive research efforts have been dedicated to the evaluation of the conditions of oil–paper composite materials, such as their aging degree and moisture content [4]. Against this background, frequency domain spectroscopy (FDS)—a non-destructive testing technology which takes

advantage of rich diagnosis information details and a strong anti-interference ability—has aroused much research interest compared with traditional methods such as Dissolved Gas Analysis or DC resistance measurement [5].

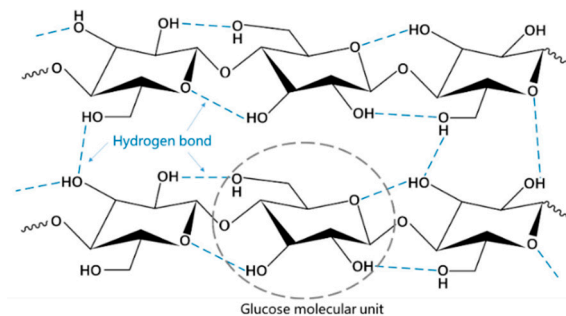


Figure 1. Molecular structure diagram of cellulose.

To enhance the estimation accuracy and universality of FDS in application, it is important to comprehensively study the microscopic generation mechanisms of the dielectric response of oil–paper material in broadband and establish a physical model of the response curves, by which sufficient characteristic parameters with definite physical meanings can be achieved, allowing insulation condition assessment to be carried out quantitatively for power equipment. It is widely accepted that the dielectric response current in an alternating electric field is led by charge motions such as polarization and conduction [6], and these motions' characteristics are significantly different in the frequency domain. For polarization, related research indicates that the relaxation polarization types with relatively long polarization times, which will cause energy loss, mainly occur in the testing frequency range of FDS (usually from 10^{-3} to 10^4 Hz) [7], and the generation of relaxation is due to the charge's barrier-hopping motions [8]; according to the dominant charge types, relaxation polarizations can be divided into space charge relaxation, interfacial relaxation, dipole relaxation and so on [9]. Meanwhile, the conduction process in dielectrics such as cellulose has been proven to be led by ions, and Dyré's work reveals that the conduction of polymers under AC voltage obeys the same mechanism as polarization, namely a trap-hopping motion of the charge [10]. Classic theoretical models such as the Debye function [11], Cole–Cole function [12] and Havriliak–Negami (H-N) function [13] were established successively to describe the single relaxation process. The quantitative expression of the conduction process under an alternating electric field has also been widely studied and applied [14]; however, when tested with a signal with a wide-frequency bandwidth, it is inevitable that the dielectric response spectrum will contain several independent dielectric processes and that these processes may overlap in some certain frequencies, which adds difficulty in understanding and analyzing the response spectrum of dielectric material. For this reason, opinions on the generation mechanisms of FDS from existing studies are divided. In [15], the FDS curve is considered to be generated by a pure conduction process in the low-frequency band, while another research work takes $\text{CaCu}_3\text{Ti}_4\text{O}_{12}$ ceramics as its experimental object and proves that a loss peak led by space charge polarization exists in the low-frequency area of complex permittivity's imaginary part spectrum, $\epsilon''(\omega)$, but is obscured by giant conduction loss [16]. Besides, although there is usually a linearly decreasing part in the low-frequency range in the spectrum of $\epsilon''(\omega)$ and it is widely considered as the result of conduction loss [17], A.K. Jonscher's research emphasizes that a special non-Debye process, called low-frequency dispersion (LFD), will also lead to a linearly decreasing trend in $\epsilon''(\omega)$, but its mechanism and frequency response characteristics are significantly different from the charge conduction [18]. Moreover, power equipment may be tested by FDS in a wide temperature range due to factors such as location, season or cooling time after ceasing operation; in this case, temperature will play an important role in determining the charge's trap-hopping motions [19]. Thus, there is no doubt that the dominant microscopic processes of a certain dielectric material's corresponding FDS curves will change if the testing temperatures are considerably different.

As stated above, there are two main purposes of the present study: the first is to realize the extraction method of the response spectra of independent dielectric processes from an oil–paper sample’s measured data with a wide testing frequency range; on this basis, the second objective is to establish the FDS curves’ function models with exact physical meanings in a wide temperature range. Section 2 discusses the basic theories of the dielectric response of materials, in which a correlation between complex permittivity’s real and imaginary parts is further determined. Section 3 introduces the present study’s experimental setups; besides FDS measurements with a series of temperatures, a thermally stimulated depolarization current test is also carried out as an auxiliary tool to provide intrinsic parameters for relaxation. Section 4 presents the measured data and provides preliminary observations. With sufficient experimental data, Section 5 presents the investigation and analysis of the dielectric processes’ independent spectra with different temperatures and further establishes their physical models. Aside from oil-impregnated cellulose paper, with its wide application background, the research thoughts developed in the present study have reference value for the spectrum analysis of other dielectric materials.

2. Theory and Deduction

2.1. Classic Model for Single Dielectric Process

In basic terms, FDS is a specific application form in the field of electrical engineering that is based on the fundamental principles of spectrum analysis, which is one of the most common material analysis approaches. Thus, classic theoretical models in dielectric physics are applicable for the explanation of the generation mechanism of FDS curves. As mentioned above, conduction and relaxation are the main causes of a material’s dielectric response. As regards the conduction process, Equation (1) describes its function expression in the frequency domain:

$$\varepsilon_{\sigma}^*(\omega) = \frac{\sigma_0}{i\omega\varepsilon_0} \quad (1)$$

where $\varepsilon_{\sigma}^*(\omega)$ stands for complex permittivity’s conduction component, σ_0 is the conductivity of dielectric material, ε_0 denotes the permittivity of a vacuum whose value is 8.85×10^{-12} F/m and ω is the angular frequency of an alternating electric field. It could be inferred from Equation (1) that the conduction process will only influence the imaginary part of a material’s complex permittivity spectrum. Moreover, in the logarithmic coordinate system, the conduction component is supposed to decrease linearly with a slope of -1 .

As regards relaxation, the Debye function, as shown in Equation (2), is the most famous physical model used to describe this process.

$$\varepsilon_r^*(\omega) = \varepsilon_{\infty} + \frac{\varepsilon_s - \varepsilon_{\infty}}{1 + i\omega\tau} \quad (2)$$

where $\varepsilon_r^*(\omega)$ is complex permittivity’s relaxation component, ε_s and ε_{∞} are known as the static dielectric constant and optical-frequency dielectric constant for the spectrum of a single relaxation process, respectively, and τ is polarization time—a key parameter related to the dominant charge’s motion characteristic. Furthermore, real and imaginary parts of $\varepsilon_r^*(\omega)$ are deduced in Equation (3) according to Equation (2).

$$\begin{cases} \varepsilon_r'(\omega) = \varepsilon_{\infty} + \frac{\varepsilon_s - \varepsilon_{\infty}}{1 + (\omega\tau)^2} \\ \varepsilon_r''(\omega) = \frac{(\varepsilon_s - \varepsilon_{\infty})(\omega\tau)}{1 + (\omega\tau)^2} \end{cases} \quad (3)$$

Based on Equation (2), further research has added extra parameters and established optimized models to solve the deviation between the measured data of relaxation and the original Debye model. Taking the H-N function as an example, its expression is presented in Equation (4),

$$\varepsilon_{HN}^*(\omega) = \varepsilon_{\infty} + \frac{\varepsilon_s - \varepsilon_{\infty}}{(1 + (i\omega\tau_{HN})^{\alpha})^{\beta}} \quad (4)$$

where parameters α and β are considered to be related to the material's structure and property.

Besides relaxation and conduction, numerous related studies have investigated another special dielectric process: in the very-low-frequency band, both $\varepsilon'(\omega)$ and $\varepsilon''(\omega)$ increase rapidly with the decrease of frequency. A.K. Jonscher specially studied this phenomenon and named it low-frequency dispersion (LFD). According to Jonscher's theory, the common relaxation process is dominated by dipole form charges, while the LFD process is dominated by the charge carrier system. When the frequency of applied voltage is relatively low, the charge carriers in dielectric material will have sufficient time to move a long distance under the action of the electric field. Quantitative investigation also revealed that LFD will cause $\varepsilon'(\omega)$ and $\varepsilon''(\omega)$ to decrease linearly in the logarithmic coordinate system, and the two corresponding curves are parallel, as shown in Equation (5).

$$\varepsilon_{LFD}'(\omega) \propto \varepsilon_{LFD}''(\omega) \propto \omega^{-\gamma} \quad (5)$$

where the range of undetermined slope coefficient γ is from 0 to 1. However, for a specific oil-impregnated cellulose paper material, the LFD process is rarely involved.

2.2. Mathematical Deduction of the Correlation between $\varepsilon'(\omega)$ and $\varepsilon''(\omega)$

As can be seen in Section 2.1, the complex permittivity is a useful parameter for describing various types of dielectric processes; thus, it is necessary to briefly explain the physical meanings of $\varepsilon'(\omega)$ and $\varepsilon''(\omega)$. For a dielectric material under applied AC voltage, its response current always contains a conductive component and capacitive component. Of these, the conductive response current has no phase difference with applied voltage, whereas there is a phase difference of 90° between the capacitive current and applied voltage. The real part of complex permittivity—namely $\varepsilon'(\omega)$ —is closely related to the capacitive current and will directly determine the material's capacitance value at the angular frequency ω . Meanwhile, the imaginary part of complex permittivity—namely $\varepsilon''(\omega)$ —could be used as an indicator for dielectric's energy loss level in the electric field considering its close relationship with the conductive response current component. It should be emphasized that the energy loss is not only caused by the charge's conduction process; as can be seen in Equation (2) and Equation (5), relaxation and LFD processes will also lead to energy loss and affect the imaginary permittivity. The conduction process has no influence on $\varepsilon'(\omega)$ and could be treated as a pure energy consumption process.

If there is a frequency range in which relaxation and conduction processes overlap, by utilizing the differences between their response spectra characteristics as mentioned above, it is possible to extract the spectrum of each independent process. According to the Debye model, the data processing approach to obtain $\varepsilon_r''(\omega)$ from $\varepsilon''(\omega)$ is deduced in Equation (6) by using first-order partial differential equation of $\varepsilon'(\omega)$.

$$\begin{aligned} -\frac{d\varepsilon'(\omega)}{d\lg\omega} &= -d\left[\varepsilon_{\infty} + \frac{\varepsilon_s - \varepsilon_{\infty}}{1 + (\omega\tau)^2}\right] / d\lg\omega = -d\left[\varepsilon_{\infty} + \frac{\varepsilon_s - \varepsilon_{\infty}}{1 + \tau^2 10^{(2\lg\omega)}}\right] / d\lg\omega \\ &= \frac{2 \ln 10}{(\varepsilon_s - \varepsilon_{\infty})} \left[\frac{(\varepsilon_s - \varepsilon_{\infty})(\omega\tau)}{1 + (\omega\tau)^2} \right]^2 = \frac{2 \ln 10}{(\varepsilon_s - \varepsilon_{\infty})} (\varepsilon_r'')^2 \end{aligned} \quad (6)$$

Substituting the exact values of parameters ε_s and ε_{∞} into Equation (6), the $\varepsilon_r''(\omega)$ spectrum led by pure relaxation process can be directly calculated according to Equation (7).

$$\varepsilon_r''(\omega) = \sqrt{(-d\varepsilon'(\omega)/d\lg\omega) / \{2 \ln 10 / [\varepsilon_s(\omega) - \varepsilon_{\infty}(\omega)]\}} \quad (7)$$

Equation (7) will play an important role below in the extraction of the independent spectrum of relaxation from overlapping bands.

3. Materials and Methods

3.1. Material Preparation

In the present study, a cellulose pressboard produced by Weidmann Company and 45# mineral oil with a freezing point of $-45\text{ }^{\circ}\text{C}$ were selected as basic materials to prepare experimental samples.

First, a pressboard with a series of thicknesses and insulating oil were separately placed in an oven under a $90\text{ }^{\circ}\text{C}$ environment for more than 48 h to remove moisture. Second, after obtaining the dried basic materials, the pressboard was dipped into mineral oil in a specific tank for another 48 h. During the immersion process, the tank was vacuumed. Finally, well-immersed oil–paper composite material was stored in a sealed condition before measurement.

3.2. Frequency Domain Spectroscopy Measurement

Concept 90, produced by Novocontrol Company, was selected as the FDS testing device. The amplitude of applied voltage was set to be 10 V while the output frequency was in the range of 10^{-3} – 10^5 Hz. Testing temperatures were adjusted by the device's own precise temperature control system. In order to obtain FDS curves in a relatively wide temperature range, oil-impregnated paper was tested from $-40\text{ }^{\circ}\text{C}$ to $100\text{ }^{\circ}\text{C}$. This precise measurement system could automatically calculate the $\epsilon'(\omega)$ and $\epsilon''(\omega)$ spectra of the test sample according to the applied voltage and response current and further provide them to the user. A diagram of the FDS measurement circuit is presented in Figure 2.

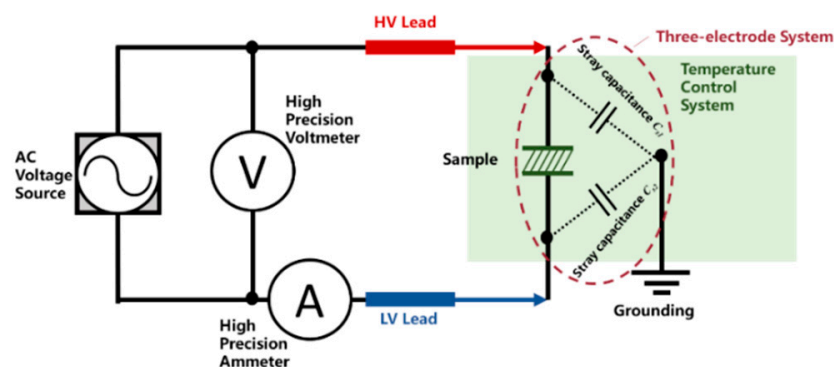


Figure 2. Diagram of the frequency domain spectroscopy (FDS) test circuit. HV: high voltage. LV: low voltage.

3.3. Thermally Stimulated Depolarization Current Measurement

Concept 80, produced by Novocontrol Company, was selected as the thermally stimulated depolarization current (TSDC) measurement device. For a complete TSDC measurement process, the oil-impregnated paper sample was first excited by a 250 V DC voltage at $50\text{ }^{\circ}\text{C}$ for 60 min to ensure that all relaxation processes were fully completed. Then, the temperature was lowered sharply to $-100\text{ }^{\circ}\text{C}$, and the excitation voltage was removed; in this way, all particle motion forms related to polarization processes were frozen. Next, the sample was heated with a constant heating rate of $5\text{ }^{\circ}\text{C}/\text{min}$, and a Keithley 6517B electrometer recorded the sample's depolarization current continuously over the entire process of increasing the temperature. According to the aims of the experiment, bias voltages were applied during the sample's depolarization process. Bias voltage values were set as -100 V , -50 V , 50 V and 100 V , respectively. The relationship between the temperature and excitation voltage for the TSDC test without bias voltage is presented in Figure 3.

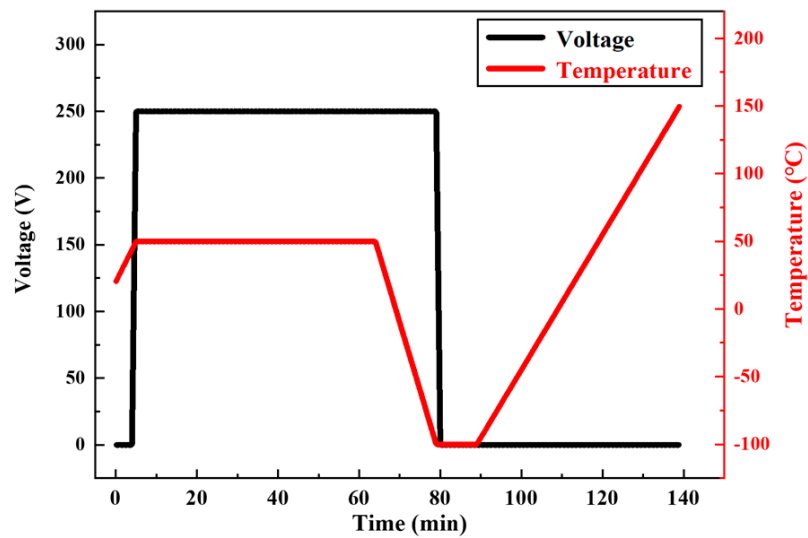


Figure 3. Applied temperature and voltage trend curve over time during the thermally stimulated depolarization current (TSDC) test.

4. Results

4.1. Experimental Data of Sample's FDS in Different Temperature Ranges

The wide temperature range is divided into three zones to present the measured FDS curves, which are the high-temperature range (80 °C to 100 °C), middle-temperature range (20 °C to 40 °C) and low-temperature range (−40 °C to −20 °C), respectively. FDS curves for samples with a thickness of 2 mm in each temperature range are shown in Figure 4. To achieve better display effects, ($\epsilon' - 1$) rather than ϵ' is selected as the vertical axis to present data related to real permittivity in the following figures.

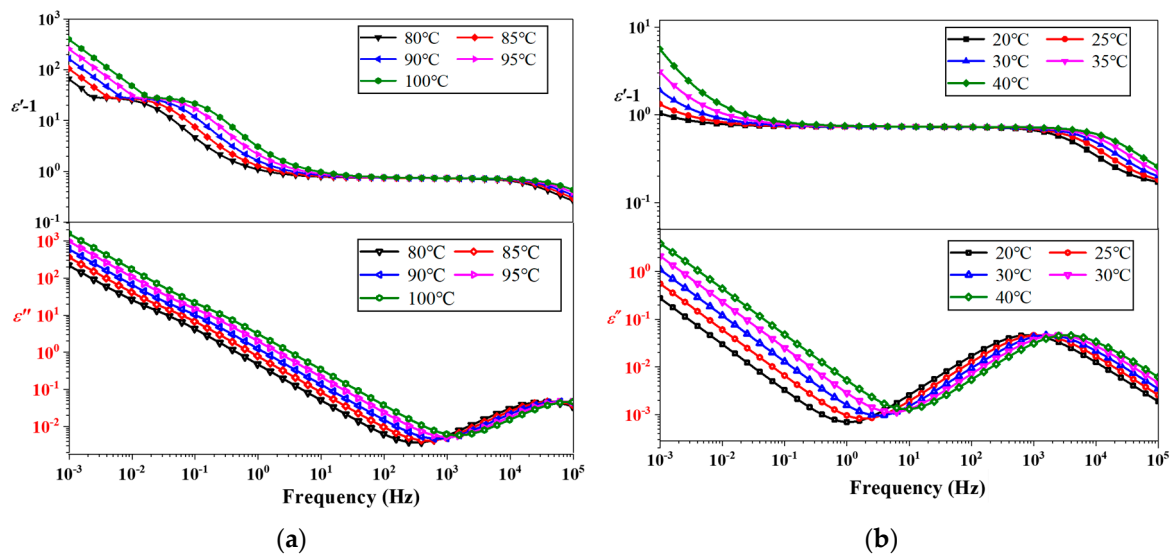


Figure 4. Cont.

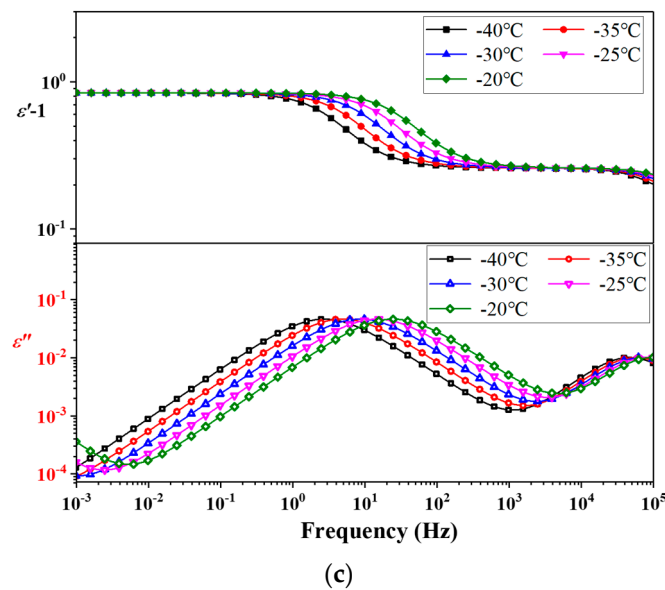


Figure 4. Measured FDS curves for the oil-impregnated cellulose paper sample in different temperature ranges: (a) FDS curves tested in the high-temperature range; (b) FDS curves tested in the middle-temperature range; (c) FDS curves tested in the low-temperature range.

Preliminary observation of Figure 4 indicates that the characteristics of FDS curves deviate significantly in different testing temperature ranges. Meanwhile, with the increase of the testing temperature, the FDS curve tends to shift to the high-frequency direction in general. These phenomena are due to the temperature's influence on the microscopic motions of the charge. Specifically, the distribution of particles that participate in trap-hopping motions obeys the Boltzmann function, and temperature is one of its key parameters, as shown in Equation (8).

$$P = \chi \cdot e^{-H/kT} \quad (8)$$

where P is a parameter related to the dielectric process, χ is an undetermined coefficient, k is called the Boltzmann constant with the value of $1.3806505 \times 10^{-23}$ J/K, T denotes the testing temperature in K and H is an important and intrinsic parameter for the dielectric process, called barrier height.

4.2. Experimental Data From Sample's TSDC Measurement

The composite dielectric sample's TSDC spectrum, as well as the fitting curves for the current peaks according to the TSDC function of relaxation, as shown in Equation (9), is presented in Figure 5.

$$I_{TSDC}(T) = \frac{p_m}{\tau_r} \exp\left[-\frac{H}{kT} - \frac{1}{R\tau_r} \int_{T_0}^T (e^{-\frac{H}{kT}}) dT\right] \quad (9)$$

where p_m is the polarization intensity in C/m^2 and R is the heating rate during the depolarization process in K/s. As can be seen, over the whole testing temperature range, there are three obvious current peaks in the TSDC spectrum, indicating three different kinds of relaxation processes. From low temperature to high temperature, the relaxation processes are marked as Relaxation A, Relaxation B and Relaxation C in turn. Moreover, based on the fitting results, the barrier heights of these three relaxation processes were obtained and are displayed in Table 1.

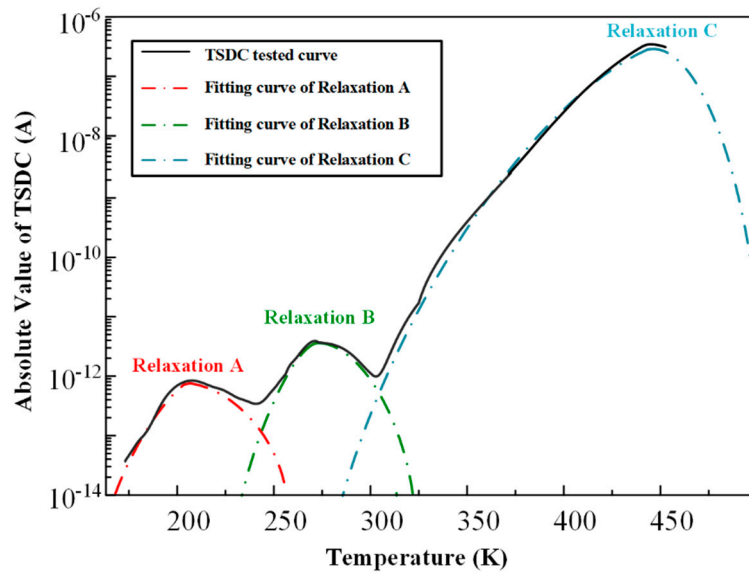


Figure 5. Measured TSDC spectrum and fitting curves for three current peaks for the oil-impregnated cellulose paper sample without bias voltage.

Table 1. Barrier heights for relaxation processes based on the fitting result of TSDC.

Process	Relaxation A	Relaxation B	Relaxation C
Barrier Height/eV	0.19	0.54	1.06

When bias voltage is applied during the heating process, according to [20], the generation mechanisms of the current peaks can be determined if the relationship between each current peak’s accumulated charge quantity and bias voltage amplitude is obtained. Take this as a reference, Figure 6 reveals each peak’s accumulated charge quantities Q_{TSDC} under different bias voltages.

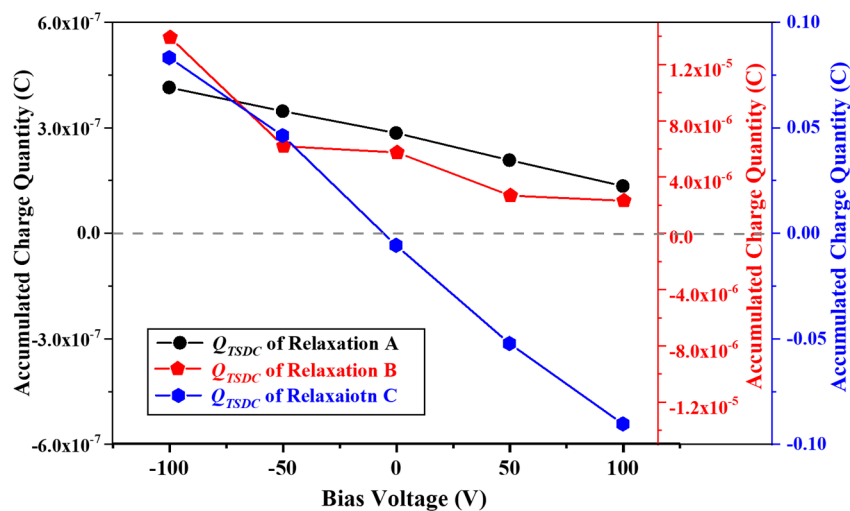


Figure 6. Relationship between accumulated charge quantity and bias voltage.

According to [21], it could be inferred from Figure 6 that the Q_{TSDC} of Relaxation A remains positive and is in a linear correlation with the bias voltage amplitude; this indicates that Relaxation A is dominated by a dipole. Meanwhile, the Q_{TSDC} of Relaxation C changes from positive to negative when the bias voltage turns to positive, the variation law of which is consistent with electrode polarization. As regards Relaxation B, the relationship between its accumulated charge quantity and

bias voltage has no obvious characteristic; thus, other criteria are needed to determine this process's generation mechanism.

5. Discussion

5.1. Mechanism Analysis and Physical Model Establishment of FDS in High-Temperature Range

In the present study, in order to fully understand the influence of various dielectric processes on the composite material's FDS curve, a synthetic analysis method based on both $\varepsilon'(\omega)$ and $\varepsilon''(\omega)$ is needed. In the lowest-frequency part of each $\varepsilon'(\omega)$ spectrum from Figure 4a, an obvious linear decline could be observed, which is supposed to be generated by a non-Debye LFD process according to Equation (5). We select data in this part and fit them linearly to the independent spectrum of the LFD process in ε' , recorded as $\varepsilon_{LFD}'(\omega)$, which could be extracted from measured $\varepsilon'(\omega)$, as shown in Figure 7, by which parameter γ in Equation (5) is calculated to be 0.912.

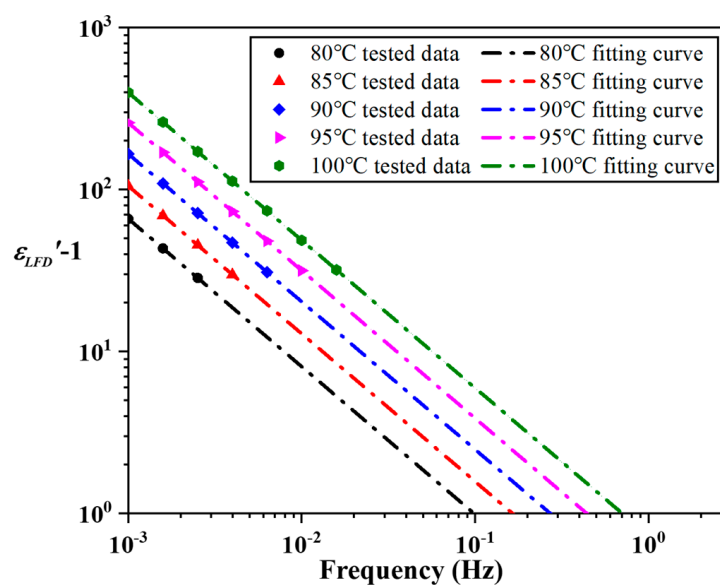


Figure 7. Extraction and fitting of real permittivity data related to the low-frequency dispersion (LFD) process.

A step-like descent appears in the higher-frequency band of $\varepsilon'(\omega)$, indicating that a Debye-form polarization occurs here. However, in the corresponding band of $\varepsilon''(\omega)$, the typical loss peak of polarization could not be investigated; instead, the measured curve shows a continuous downward trend. To obtain the independent spectrum of this relaxation process in the permittivity's imaginary part, the deduction made in Section 2.2—namely Equation (7)—is necessary to apply here. By substituting the values of parameters ε_s and ε_∞ , which could be directly acquired from Figure 4a, the relaxation's spectra, expressed by ε'' in a frequency range from approximately 10^{-3} to 10^1 , at high temperatures are calculated and shown in Figure 8a; all the curves are in the ideal peak shape. Furthermore, the barrier height of the relaxation process presented in Figure 8 could be obtained according to Equation (8)—as also shown in Figure 8a—and its value is fitted to be 1.05 eV. Essentially, FDS and TSDC are testing methods for a material's microscopic dielectric processes from different perspectives, and barrier height could be used as a key parameter to establish a linkage between them. According to the data in Table 1, it could be inferred that the spectra in Figure 8a describe the same relaxation process as Relaxation C in Figure 5, which means that the relaxation that occurs at low frequency in the FDS spectra in Figure 4a is electrode polarization.

Electrode polarization is led by space charges that accumulate in near-electrode regions [22]. With the use of an electrical field, particles will form charge layers that are opposite to the electrodes'

polarities; layers next to the anode and cathode lead to the appearance of the electric moment and further cause a polarization phenomenon. Based on this mechanism, the electrode relaxation’s polarization time, τ_{er} , is decided by the distance between the anode and cathode, which is equal to the sample’s thickness in the present study, considering that panel electrodes are utilized for FDS measurement. The theoretical formula of τ_{er} is expressed in Equation (10).

$$\tau_{er} = \frac{L}{2\mu} \sqrt{\frac{\epsilon_r \epsilon_0}{p_0 k T}} \tag{10}$$

where L stands for the sample’s thickness in this case, μ denotes the charge mobility and ϵ_r is the dielectric’s relative permittivity, whose value is usually greater than 1. This relationship indicates that, for electrode relaxation, the parameter τ_{er} is proportional to the sample’s thickness. To verify this, oil–paper composite dielectric samples with thicknesses of 500 μm , 1 mm and 2 mm were additionally tested by FDS. The measured curves and their processed results are shown in Figure 8b–d in turn as examples. As can be seen, the fitting curve in Figure 8d coincides with Equation (10), which could be treated as further evidence of the inference of the generation mechanism of this relaxation process.

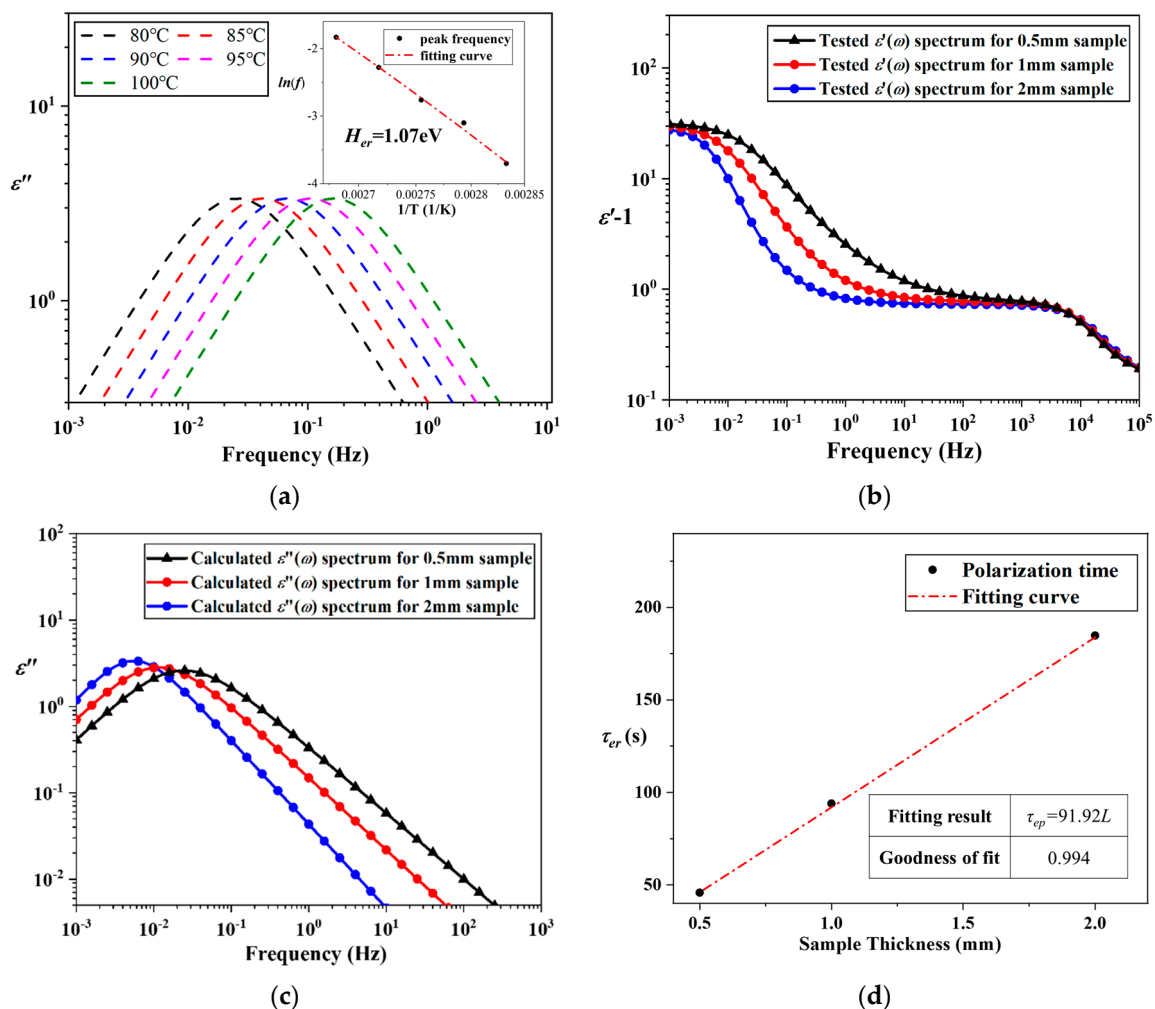


Figure 8. Related analysis data for electrode relaxation. (a) Extracted $\epsilon''(\omega)$ spectra of electrode relaxation at different temperatures, and fitting result of the electrode relaxation’s barrier height. (b) Measured $\epsilon'(\omega)$ spectra of composite samples with different thicknesses. (c) Calculated electrode relaxation independent $\epsilon''(\omega)$ spectra for samples with different thicknesses. (d) Relationship between sample thickness and electrode relaxation’s polarization time.

By subtracting the electrode relaxation loss—namely $\varepsilon_{er}''(\omega)$ —in Figure 8a from the measured curve of $\varepsilon''(\omega)$, this process's influence on imaginary permittivity could be effectively eliminated. Related data processing results are shown in Figure 9. As can be seen, the remainder varies linearly with frequency in the logarithmic coordinate system. It can be further observed that the average slope of the data in Figure 9 is -0.962 . In the low-frequency band, according to the theoretical models, the impacts of the conduction process described by Equation (1) and low-frequency dispersion process described by Equation (5)—in which the parameter γ is equal to 0.912—are both supposed to be significant due to their negative correlation with the applied electric field's frequency. As a result, the composite spectrum of these two linear processes is still supposed to be a descending line, and its slope in theory should be -0.956 , the slope of the average value of conduction should be -1 and the slope of LFD should be -0.912 . In this respect, the slopes of measured data shown in Figure 9 coincide very well with the theoretical values, indicating that the low-frequency part of the composite sample's FDS curve consists of three independent dielectric processes, which are low-frequency dispersion, conduction and electrode relaxation, respectively.

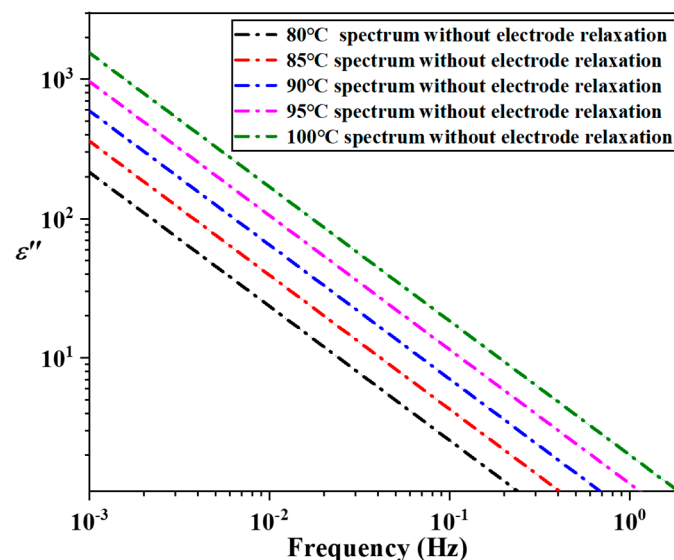


Figure 9. Compound spectra for linear conduction and LFD processes in a high-temperature range.

When reaching the high-frequency range, curves with obvious characteristics of Debye-type relaxation can be observed in both $\varepsilon'(\omega)$ and $\varepsilon''(\omega)$ in Figure 4a. Furthermore, because of the inverse relationship between the frequency and loss levels of both conduction and LFD processes, the emerging relaxation process takes a dominant position in this band. Thus, this new relaxation process could be fitted by experimental data directly without further processing, as shown in Figure 10a. Besides fitting curves, the barrier height of this dielectric process is also obtained, which is 0.56 eV. By comparison with the data in Table 1, it could be inferred that the high-frequency relaxation in Figure 10a and Relaxation B in Figure 5 are the same process tested by different approaches. In order to determine the generation mechanism of this kind of high-frequency relaxation, an as-received cellulose pressboard sample without an immersion process was additionally tested by FDS. The differences between the FDS curves of oil-impregnated pressboard and as-received pressboard are shown in Figure 10b; as can be seen, a phenomenon related to Debye-form relaxation could be observed in neither $\varepsilon'(\omega)$ nor $\varepsilon''(\omega)$ of as-received pressboard. According to this, the type of high-frequency relaxation for the composite sample tested in a high-temperature range is considered to be interfacial relaxation.

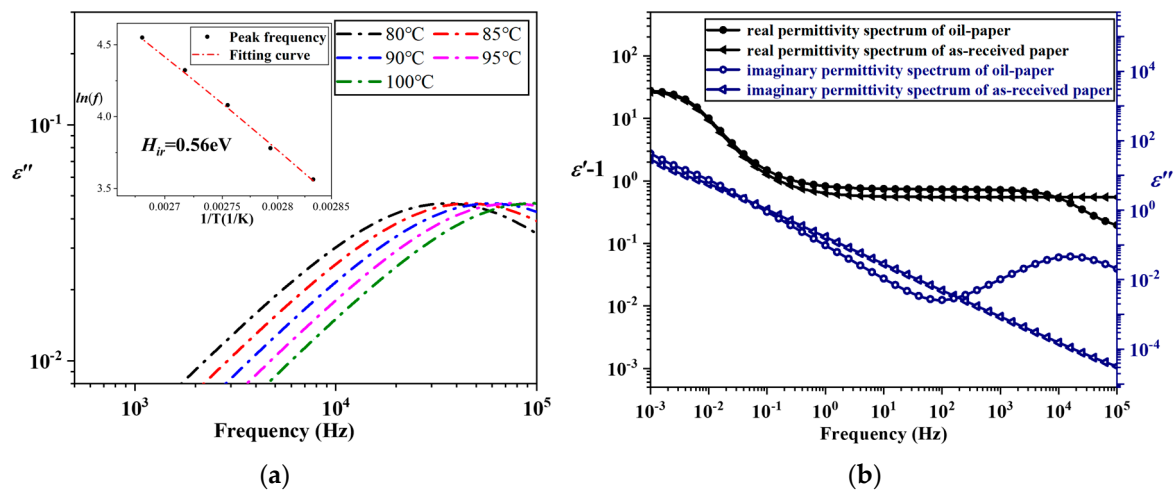


Figure 10. Related experimental data and analysis of the interfacial relaxation of the oil–paper sample in a high-temperature range. (a) Independent spectra of interfacial relaxation under different temperatures. (b) FDS comparisons between as-received cellulose paper and oil–paper composite sample.

Interfacial relaxation is a special kind of relaxation in composite dielectric materials. According to the Maxwell–Wagner effect [23], charges will accumulate upon the interlayer of two kinds of dielectric materials—cellulose and mineral oil in this case—as their dielectric constants are significantly different, which will further lead to the formation of an electric moment. Strictly speaking, interfacial relaxation could also be treated as a special kind of space charge relaxation, but its relaxation time is much shorter than electrode relaxation. Although existing studies have observed this process in oil–paper samples several times [24,25], its microscopic mechanism has not been discussed in depth before.

Considering the analysis above, it could be concluded that, in the high-temperature range, the whole FDS curve of oil–paper composite material could be treated as a combination of low-frequency dispersion, conduction, electrode relaxation and interfacial relaxation; according to the theoretical expression of each independent process, Figure 11 establishes the physical model of broadband $\epsilon''(\omega)$ spectrum in the high-temperature range by taking data tested at 80 °C as an example. The reason for selecting $\epsilon''(\omega)$ is that all dielectric processes have influences on it.

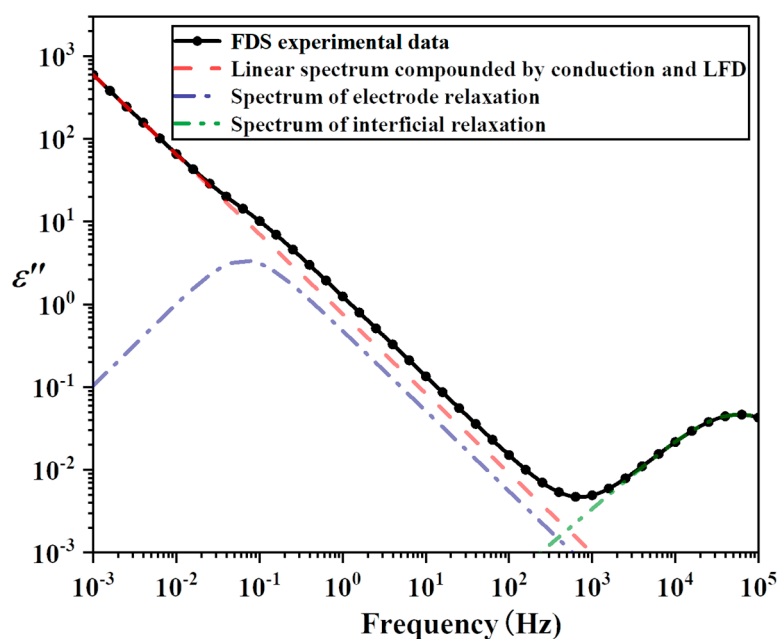


Figure 11. Physical model of FDS tested in a high-temperature range.

5.2. Mechanism Analysis and Physical Model Establishment on FDS in Middle-Temperature Range

The characteristics of FDS curves in the middle-temperature range are quite different from those in the high-temperature range, as can be seen in Figure 4b. In the low-frequency range of $\varepsilon'(\omega)$, a linear descent part could no longer be observed, which means that the LFD process's influence on $\varepsilon'(\omega)$ is greatly weakened. Moreover, although the low-frequency part of $\varepsilon'(\omega)$ shows a downward trend, there is no relaxation peak in the corresponding band of $\varepsilon''(\omega)$, indicating that several independent dielectric processes may overlap in this band and the relaxation process is obscured. Using a processing method similar to Section 5.1 on the low-frequency data of $\varepsilon'(\omega)$ and $\varepsilon''(\omega)$ spectra according to Equation (7), independent relaxation spectrum can be extracted, as shown in Figure 12a. Furthermore, the barrier height is calculated to be 1.05 eV—almost the same as the barrier height value of the relaxation process presented in Figure 8a—indicating that the relaxation process in Figure 12a is also generated by space charges near the electrode area.

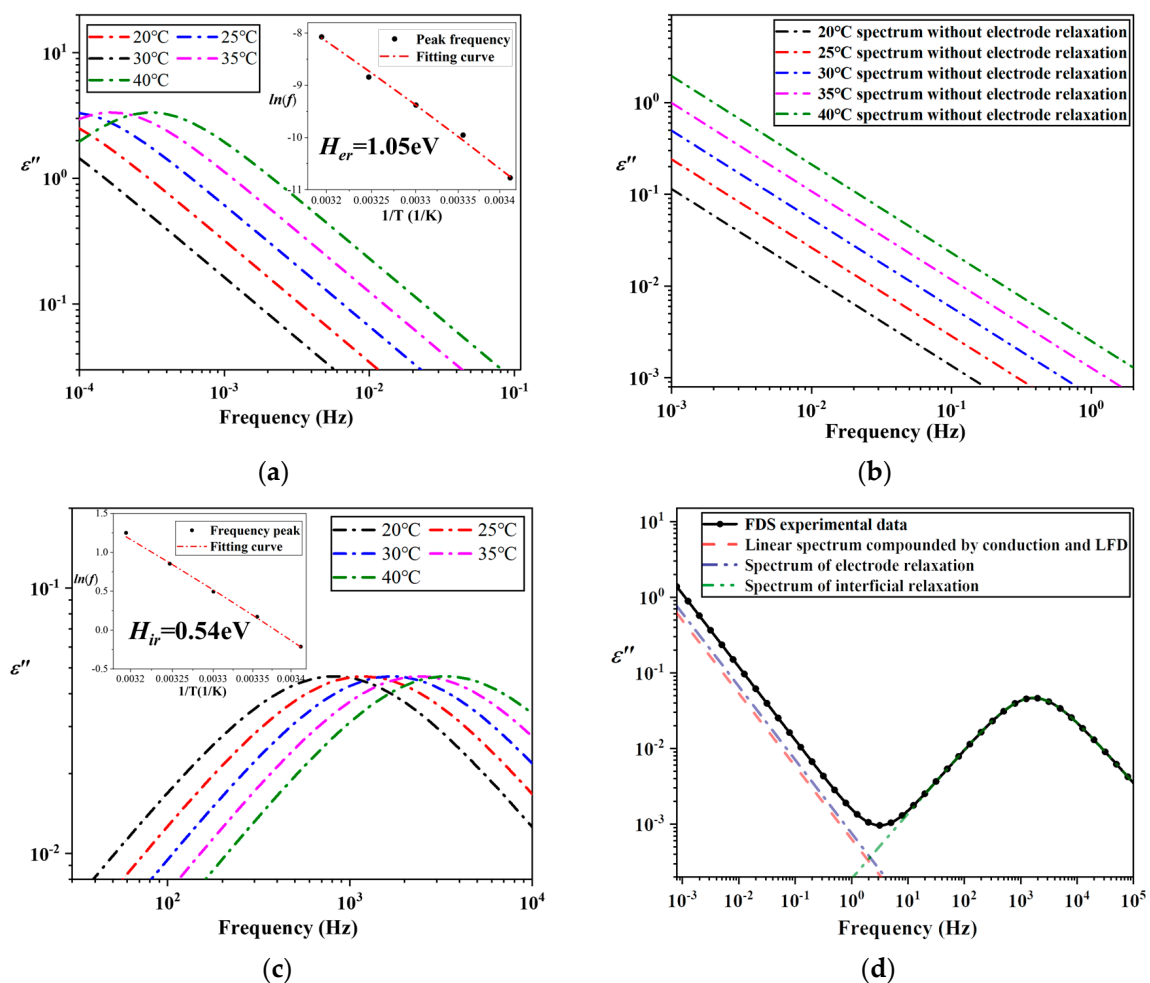


Figure 12. Data analysis for FDS tested in the middle-temperature range. (a) Independent spectra for electrode relaxation in the middle-temperature range. (b) Compound spectra for linear conduction and LFD processes in the middle-temperature range. (c) Independent spectra for interfacial relaxation in the middle-temperature range. (d) Physical model of FDS tested in the middle-temperature range.

By subtracting the corresponding electrode relaxation loss spectra in Figure 12a, the remainder of each measured $\varepsilon''(\omega)$ spectrum also has a linear relationship with the logarithmic value of frequency, as shown in Figure 12b. The average slope value of the spectra in Figure 12b is calculated to be -0.958 —almost equal to the slope in Figure 9. If the FDS measurement for the oil–paper composite material in the high-temperature range were not carried out in Section 3.2, after eliminating the influence of electrode relaxation, the remaining linear spectra in Figure 12b may be easily considered to be led only by the conduction process; however, according to the detailed analysis of the LFD process, as can be seen in Section 2.1, it could be inferred that the difference between the data slope of -0.958 and the theoretical slope of conduction is not due to a data processing error but to the existence of the LFD process, although this is not clearly observed in the $\varepsilon''(\omega)$ spectrum of the middle-temperature range.

In the higher-frequency range of each $\varepsilon''(\omega)$ spectrum in Figure 4b, an obvious relaxation peak can be directly observed; a step-like descent appears in the $\varepsilon'(\omega)$ spectrum in the same band. Independent spectra of this process in the middle-temperature range are fitted and presented in Figure 12c. The calculated barrier height value is 0.54 eV, indicating that this process is led by charges that accumulated in the sample's solid–liquid interface.

In summary, the $\varepsilon''(\omega)$ spectra in the middle-temperature range could be treated as a combination of the LFD process, conduction, electrode relaxation and interfacial relaxation. A physical model based on this generation mechanism is established in Figure 12d.

5.3. Mechanism Analysis and Physical Model Establishment on FDS in Low-Temperature Range

Preliminary observation of the measured data from Figure 4c indicates that the curve characteristics in the low-temperature range differ a great deal from the spectra in the other two temperature ranges. In the $\varepsilon''(\omega)$ spectra, instead of a dominated linear decline in the low-frequency range, two typical relaxation peaks could be observed directly in the whole tested band. Correspondingly, the real part of complex permittivity remains almost unchanged until the applied voltage frequency exceeds 10^0 Hz; besides this, two step-like descents could be also observed in the bands where relaxation peaks occur in $\varepsilon''(\omega)$.

The above phenomena indicate that dielectric processes with linear spectra—namely conduction and LFD processes—no longer affect the oil–paper composite material's FDS curve at very low temperatures. Instead, the dominant processes become two different kinds of relaxation. To quantitatively analyze the two processes, respectively, data of the relaxation peaks are directly fitted without extra steps. As can be seen in Figure 13a,b, the barrier heights of the relaxation process in the middle-frequency band and high-frequency band are 0.57 eV and 0.17 eV, respectively. By comparing these barrier height values with the data in Table 1, it could be inferred that the process in Figure 13a is interfacial relaxation, while the process in Figure 13b is dipole relaxation. Dipole relaxation is one of the most common relaxation types; however, as its relaxation time is much shorter than that of electrode relaxation or interfacial relaxation, in the general measurement frequency band of FDS, the relaxation peak generated by dipole relaxation will not appear until the sample's temperature drops to a very low value.

Based on the two relaxation processes' independent spectra functions, the physical model for the FDS of the oil–paper composite material in the low-temperature range is established in Figure 13c.

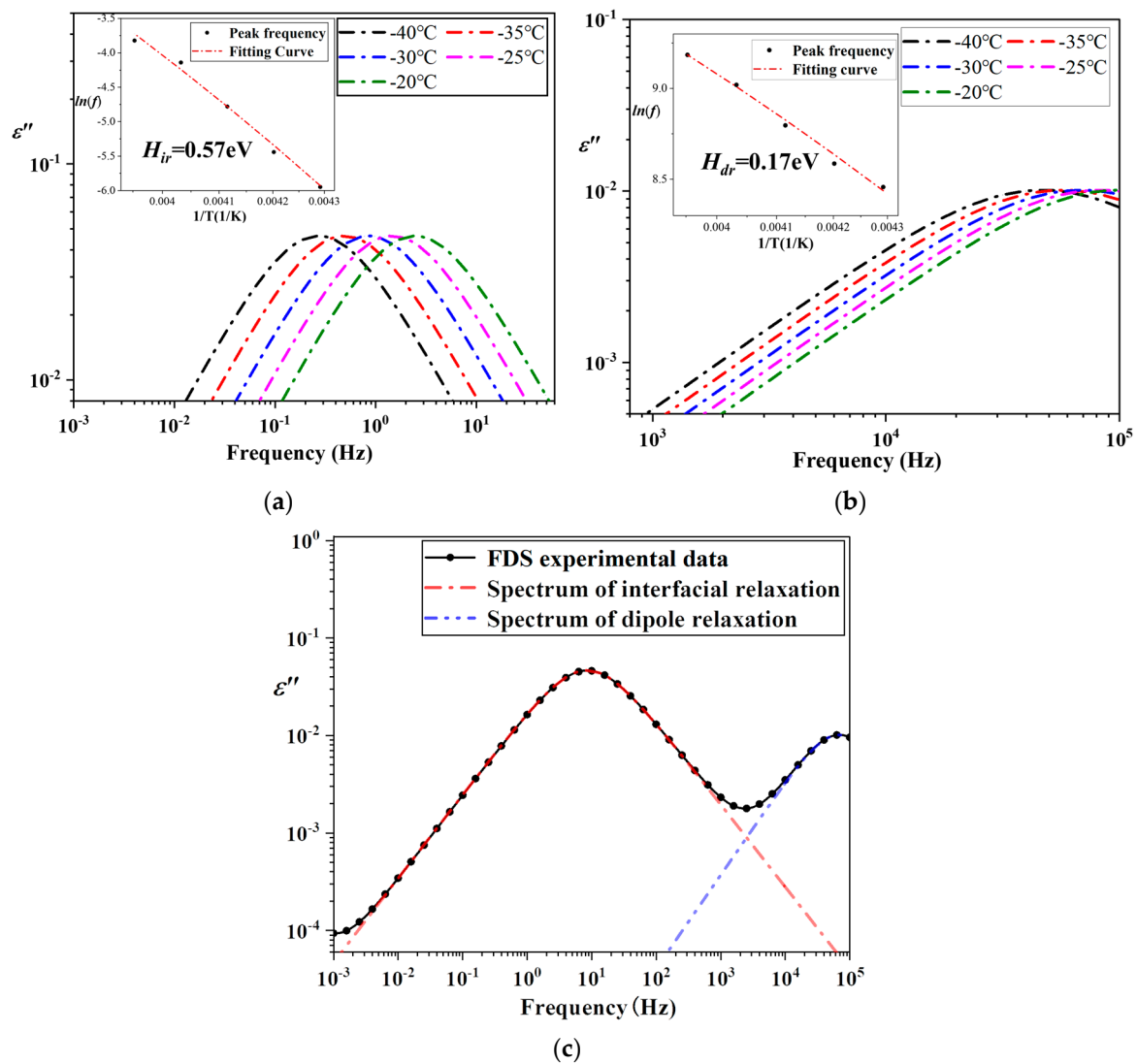


Figure 13. Data analysis for FDS tested in the low-temperature range. (a) Independent spectra for interfacial relaxation in the low-temperature range. (b) Independent spectra for dipole relaxation in the low-temperature range. (c) Physical model of FDS tested in the low-temperature range.

5.4. Abstraction of Oil–Paper Composite Material FDS Function Models in Different Temperature Ranges

According to the discussions above, the microscopic generation mechanisms of the broadband dielectric response spectra of composite materials whose testing temperatures are significantly different have been compared and clarified. On this basis, abstract physical models in a wide temperature range can be summarized.

For FDS in the high-temperature range, the LFD process, electrode relaxation, conduction and interfacial relaxation are all clearly reflected; thus, its physical model could be expressed as Equation (11).

$$\epsilon_{HT}^*(\omega) = \epsilon_{LFD}^*(\omega) + \epsilon_{\sigma}^*(\omega) + \epsilon_{er}^*(\omega) + \epsilon_{ir}^*(\omega) \tag{11}$$

For FDS in the middle-temperature range, the LFD process is greatly weakened and not reflected in $\epsilon'(\omega)$, but it still affects the $\epsilon''(\omega)$ significantly. Thus, the physical model for FDS in this temperature range could be expressed as Equation (12).

$$\begin{cases} \epsilon'_{MT} = \epsilon'_{er} + \epsilon'_{ir} \\ \epsilon''_{MT} = \epsilon''_{LFD} + \epsilon''_{\sigma} + \epsilon''_{er} + \epsilon''_{ir} \end{cases} \tag{12}$$

As regards the low-temperature range, the composite sample's FDS curves in this range are dominated by interfacial relaxation and dipole relaxation over the whole band. Thus, its physical model could be expressed as Equation (13).

$$\varepsilon_{LT}^* = \varepsilon_{ir}^* + \varepsilon_{dr}^* \quad (13)$$

6. Conclusions

As an important material analysis method, as well as a useful tool in terms of engineering applications, dielectric spectroscopy in the frequency domain is affected by temperature to a great extent. Thus, in a wide temperature range, the dominant microscopic processes of FDS change, and the measured curves' macroscopic characteristics are significantly different. In the present study, a comprehensive FDS analysis method for an oil–paper composite material that synthetically and quantitatively takes multiple parameters, such as ε' , ε'' , the first-order partial differential equation of $\varepsilon'(\omega)$ and the sample's TSDC spectrum, into consideration is developed, based on which the spectra of independent dielectric processes under different temperatures are effectively extracted, and their generation mechanisms are also verified from various perspectives. Further, quantitative models for FDS in different temperature ranges with exact physical meanings are established. Specific conclusions are summarized as follows.

- (a) In the low-frequency part of the $\varepsilon''(\omega)$ spectra with medium or high testing temperatures, LFD, conduction and electrode relaxation processes overlap. Of these, both LFD and conduction have linear spectra. Moreover, the relaxation time of electrode relaxation with a barrier height of 1.05 eV is in direct proportion to the sample's thickness.
- (b) The dielectric process with a barrier height of about 0.56 eV—which mainly occurs in the high-frequency range when the sample is in the high or middle-temperature ranges or in the middle-frequency range at low temperatures—is inferred to be interfacial relaxation, which is a typical process for a composite material with clear interface layers.
- (c) When the FDS test is carried out in the low-temperature range, a dipole relaxation peak with a barrier height of 0.19 eV will dominate the high-frequency range of the oil–paper composite material's FDS curve.

Author Contributions: Conceptualization, J.X. and K.Y.; methodology, J.X.; validation, K.X., Y.H. and C.X.; formal analysis, J.X.; investigation, J.X., M.D. and B.Y.; resources, Y.H.; data curation, M.D. and B.Y.; writing—original draft preparation, J.X.; writing—review and editing, M.D. and B.Y.; visualization, J.X.; supervision, J.X.; project administration, K.Y.; funding acquisition, Y.H. All authors have read and agreed to the published version of the manuscript.

Funding: This research was funded by the Natural Science Foundation of China, grant no. U1866603 and 51877171, and the National Key Research and Development Program of China, grant no. 2017YFB0902705).

Conflicts of Interest: The authors declare no conflict of interest.

References

1. Nie, H.; Wei, X.; Wang, Y.; Chen, Q. A Study of Electrical Aging of the Turn-to-Turn Oil-Paper Insulation in Transformers with a Step-Stress Method. *Energies* **2018**, *11*, 3338. [[CrossRef](#)]
2. Li, Y.; Zhong, L.; Yu, Q.; Zhang, C.; Jiang, S.; Xue, F.; Li, H.; Zhao, Y. Influence of moisture content on cellulose structure and breakdown strength of vegetable oil-impregnated paper. *IEEE Trans. Dielectr. Electr. Insul.* **2019**, *26*, 1245–1252. [[CrossRef](#)]
3. Yang, F.; Du, L.; Yang, L.; Wei, C.; Wang, Y.; Ran, L.; He, P. A Parameterization Approach for the Dielectric Response Model of Oil Paper Insulation Using FDS Measurements. *Energies* **2018**, *11*, 622. [[CrossRef](#)]
4. Xie, J.; Dong, M.; Xu, G.; Hu, Y.; Yang, K.; Xia, C.; Wang, B. Quantitative aging assessment method for cellulose pressboard based on the interpretation of the dielectric response mechanism. *Cellulose* **2020**, *27*, 4773–4785. [[CrossRef](#)]

5. Xia, G.; Wu, G.; Gao, B.; Yin, H.; Yang, F. A New Method for Evaluating Moisture Content and Aging Degree of Transformer Oil-Paper Insulation Based on Frequency Domain Spectroscopy. *Energies* **2017**, *10*, 1195. [[CrossRef](#)]
6. Ekanayake, C.; Gubanski, S.; Graczkowski, A.; Walczak, K. Frequency response of oil impregnated pressboard and paper samples for estimating moisture in transformer insulation. *IEEE Trans. Power Del.* **2006**, *21*, 1309–1317. [[CrossRef](#)]
7. Chatterjee, S.; Pradhan, A.; Dalai, S.; Chatterjee, B.; Chakravorti, S. Reducing frequency domain spectroscopy measurement time for condition monitoring of transformer oil-paper insulation using non-sinusoidal excitations. *IET Sci. Meas. Technol.* **2017**, *11*, 204–212. [[CrossRef](#)]
8. Hino, T. Thermally stimulated characteristics in solid dielectrics. *IEEE Trans. Dielectr. Electr. Insul.* **1980**, *15*, 301–311. [[CrossRef](#)]
9. Zhao, S. *Dielectric Spectroscopy Method and Application*; Chemical Industry Press: Beijing, China, 2008.
10. Fleetwood, D.; Reber, R.; Winokur, P. Effect of bias on thermally stimulated current (TSC) in irradiated mos devices. *IEEE Trans. Nucl. Sci.* **1991**, *38*, 1066–1077. [[CrossRef](#)]
11. Baral, A.; Chakravorti, S. Condition assessment of cellulosic part in power transformer insulation using transfer function zero of modified debye model. *IEEE Trans. Dielectr. Electr. Insul.* **2014**, *21*, 2028–2036. [[CrossRef](#)]
12. Wolny, S.; Adamowicz, A.; Lepich, M. Influence of Temperature and Moisture Level in Paper-Oil Insulation on the Parameters of the Cole-Cole Model. *IEEE Trans. Power Deliv.* **2014**, *29*, 246–250. [[CrossRef](#)]
13. Hadjadj, Y.; Meghnefi, F.; Fofana, I.; Ezzaidi, H. On the Feasibility of Using Poles Computed from Frequency Domain Spectroscopy to Assess Oil Impregnated Paper Insulation Conditions. *Energies* **2013**, *6*, 2204–2220. [[CrossRef](#)]
14. Wang, L.; Dong, M.; Dai, J.; Ma, A.; Xie, J.; Wang, K. Aging characteristic parameter extraction of oil-paper insulation based on frequency domain spectroscopy. In Proceedings of the 2016 International Conference on Condition Monitoring and Diagnosis (CMD), Xi'an, China, 25–28 September 2016; pp. 968–971.
15. Dong, M.; Ren, M.; Wen, F.; Zhang, C.; Liu, J.; Christof, S.; Michael, M. Explanation and analysis of oil-paper insulation based on frequency-domain dielectric spectroscopy. *IEEE Trans. Dielectr. Electr. Insul.* **2015**, *22*, 2684–2693. [[CrossRef](#)]
16. Wu, K.; Huang, Y.; Li, J.; Li, S. Space charge polarization modulated instability of low frequency permittivity in CaCu₃Ti₄O₁₂ ceramics. *Appl. Phys. Lett.* **2017**, *111*, 042902. [[CrossRef](#)]
17. Bandara, K.; Ekanayake, C.; Saha, T. Analysis of frequency domain dielectric response of pressboard insulation impregnated with different insulating liquids. *IEEE Trans. Dielectr. Electr. Insul.* **2016**, *23*, 2042–2050. [[CrossRef](#)]
18. Jonscher, A. *Dielectric Relaxation in Solids*; Chelsea Dielectrics Press: London, UK, 1983.
19. Liu, J.; Fan, X.; Zhang, Y.; Zheng, H.; Yao, H.; Zhang, C.; Zhang, Y.; Li, D. A Novel Universal Approach for Temperature Correction on Frequency Domain Spectroscopy Curve of Transformer Polymer Insulation. *Polymers* **2019**, *11*, 1126. [[CrossRef](#)]
20. Wang, S.; Zhang, G.; Wei, J.; Yang, S.; Dong, M. Investigation on dielectric response characteristics of thermally aged insulating pressboard in vacuum and oil-impregnated ambient. *IEEE Trans. Dielectr. Electr. Insul.* **2010**, *17*, 1853–1862. [[CrossRef](#)]
21. Xie, J.; Dong, M.; Hu, Y.; Zhuang, T.; Albarracín-Sánchez, R.; Johnatan, M. Modeling oil-paper insulation frequency domain spectroscopy based on its microscopic dielectric processes. *IEEE Trans. Dielectr. Electr. Insul.* **2019**, *26*, 1788–1796. [[CrossRef](#)]
22. Chen, R.; Krish, Y. *Analysis of Thermally Stimulated Processes*; Pergamon Press: Oxford, UK, 1981; pp. 15–24.
23. Zhu, Y.; Li, S.; Min, D. Origin of dielectric processes in aged oil impregnated paper. *IEEE Trans. Dielectr. Electr. Insul.* **2017**, *24*, 1625–1635. [[CrossRef](#)]
24. Havriliak, S.; Negami, S. A complex plane representation of dielectric and mechanical relaxation processes in some polymers. *Polymer* **1967**, *8*, 161–210. [[CrossRef](#)]
25. Li, S.; Zhu, D.; Min, D.; Chen, G. Space Charge Modulated Electrical Breakdown. *Sci. Rep.* **2016**, *6*, 32588. [[CrossRef](#)] [[PubMed](#)]

